Materials and Design 32 (2011) 4665–4675

Contents lists available at ScienceDirect

Materials and Design

journal homepage: www.elsevier.com/locate/matdes

Mechanical properties of additive manufactured titanium (Ti–6Al–4V) blocks deposited by a solid-state laser and wire

Erhard Brandl [a,*], Frank Palm [a], Vesselin Michailov [b], Bernd Viehweger [c], Christoph Leyens [d]

[a] EADS Innovation Works, Metallic Technologies & Surface Engineering, D-81663 Munich, Germany
[b] Brandenburg University of Technology Cottbus, Chair of Joining and Welding Technology, Konrad-Wachsmann-Allee 17, D-03046 Cottbus, Germany
[c] Brandenburg University of Technology Cottbus, Chair of Design and Manufacturing, Konrad-Wachsmann-Allee 1, D-03046 Cottbus, Germany
[d] Technical University of Dresden, Institute of Materials Science, Chair of Materials Technology, Berndt-Bau, Helmholtzstr. 7, D-01062 Dresden, Germany

ARTICLE INFO

Article history:
Received 11 April 2011
Accepted 27 June 2011
Available online 2 July 2011

Keywords:
A. Non-ferrous metals and alloys
E. Mechanical
F. Microstructure

ABSTRACT

In this paper, the mechanical properties and chemical composition of additive manufactured Ti–6Al–4V blocks are investigated and compared to plate material and aerospace specifications. Blocks (seven beads wide, seven layers high, 165 mm long) were deposited using a 3.5 kW Nd:YAG laser and Ti–6Al–4V wire. Two different sets of process parameters are used and three different conditions (as-built, 600 °C/4 h, 1200 °C/2 h) of the deposit are investigated. The particular impurity levels of the blocks are considerably below those tolerated according to aerospace material specifications (AMS 4911L). Static tensile samples are extracted from the blocks in the deposition direction and punch samples are extracted in the building direction. The experiments show that as-deposited Ti–6Al–4V can achieve strength and ductility properties that fulfill aerospace specifications of the wrought Ti–6Al–4V material (AMS 4928). The 600 °C/4 h heat treatment leads to a significantly higher strength in the deposition direction, but can also decrease ductility. The 1200 °C/2 h treatment tends to decrease the alloy's strength.

1. Introduction

Ti–6Al–4V is the most common titanium alloy and one of the most common aerospace alloys [1–3]. Ti–6Al–4V aerospace components are mostly machined from costly wrought material at a high buy-to-fly ratio. Therefore, additive layer manufacturing (ALM) processes, which manufacture near-net-shape components at a low buy-to-fly ratio, are of great economical and ecological interest. All additive layer manufacturing technologies share the layer-additive approach (Fig. 1): A three-dimensional computer-aided design (CAD) model is sliced into thin layers. With the slice file, this particular ALM process builds the physical part layer by layer.

Additive layer manufacturing includes four processing routes as illustrated in Table 1.

Most additive manufactured Ti–6Al–4V parts are built up from powderized feedstock in a powder-bed or powder-feed (also: blown powder) process [5]. However, aerospace components require high material quality and high repeatability. Wire has generally a higher purity of the starting feedstock than powder and is less susceptible to contamination during the process due to its reduced surface area [6,7]. Further advantages of wire feedstock include high deposition efficiency, high deposition rate, good availability and simplified handling and storage. For these reasons, recent research activities [8–18] have focused on processes using Ti–6Al–4V wire feedstock instead of powder. For detailed research in this field, a wire-feed ALM process was established and blocks were deposited. In the present paper, the mechanical properties of such Ti–6Al–4V deposits and their chemical composition are investigated and evaluated from an aerospace point of view.

2. Experimental methods

2.1. Wire-feed process

The wire-feed process basically consists of a neodymium-doped yttrium aluminium garnet (Nd:YAG, wavelength $\lambda = 1064$ nm) laser with 3.5 kW maximum power, a 6-axis robot, and a lateral wire-feeding device. Ti–6Al–4V wire with extra low interstitials (ELI) is deposited onto a Ti–6Al–4V plate (6.35 mm thick). The process takes place in an open box that is permanently flooded by argon from its base. The setup and the process are described comprehensively elsewhere [4]. A schematic drawing of the process is shown in Fig. 2.

* Corresponding author. Tel.: +49 (0)89 607 22107; fax: +49 (0)89 607 25408.
E-mail addresses: erhard.brandl@eads.net (E. Brandl), frank.palm@eads.net (F. Palm), michailov@tu-cottbus.de (V. Michailov), viehweger@kuf.tu-cottbus.de (B. Viehweger), christoph.leyens@tu-dresden.de (C. Leyens).

0261-3069/$ - see front matter © 2011 Elsevier Ltd. All rights reserved.
doi:10.1016/j.matdes.2011.06.062

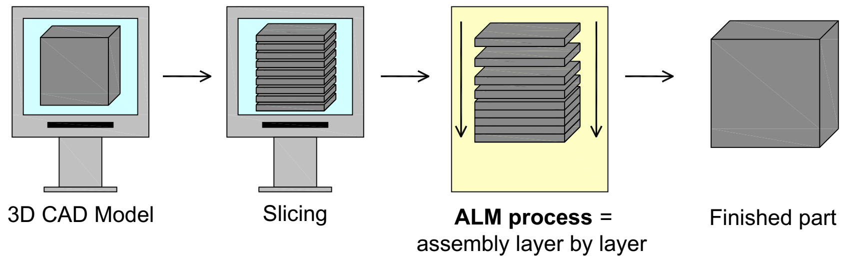

Fig. 1. Schematic sequence of additive layer manufacturing (ALM).

Table 1
Classification of the additive layer manufacturing processing routes [4].

	Additive layer manufacturing (ALM) processes						
Process	Powder-bed		Powder-feed	Wire-feed			Others
Heat source	Laser beam	Electron beam	Laser beam	Laser beam	Arc beam	Electron beam	E.g. cold gas spray
Advantage	+Part complexity		+Material variety		+Deposition rate		+Low heat input
Disadvantage	−Deposition rate		−Deposition efficiency		−Part complexity		−Part complexity

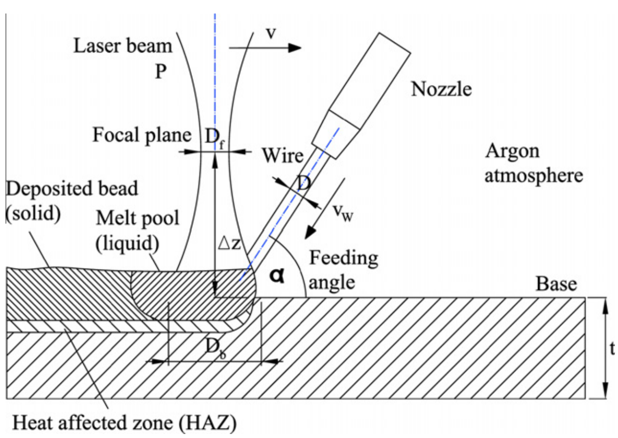

Fig. 2. Schematic drawing of the wire-feed deposition process used for the manufacture of the Ti–6Al–4V blocks.

Table 2
Details of the wire-feed deposition setup and process parameter sets (P38, P58) used for the manufacture of the Ti–6Al–4V blocks.

	Abbreviation	Unit	Parameter set P38	Parameter set P58
Laser power	P	(kW)	3.5	2.625
Deposition or welding speed	v	(mm/s)	10	7.5
Wire-feed speed	v_W	(mm/s)	40	30
Wire-feed speed factor	$k = v_W/v$	[1]	4	4
Heat input per unit length of weld	P/v	(J/mm)	350	350
Diameter of optical fibre		(mm)	0.4	
Focal length of optics		(mm)	140	
Focal plane diameter	D_f	(mm)	0.56	
Focal position	Δz	(mm)	23	
Diameter of beam at surface of base	D_b	(mm)	~ 4.1	
Thickness of Ti–6Al–4V base	t	(mm)	6.35	
Diameter of Ti–6Al–4V wire	D	(mm)	1.2	
Feeding angle	α	(°)	55	

Details of the parameter sets and experimental settings are listed in Table 2. Two different deposition parameter sets (P38, P58) were used.

2.2. Deposition of blocks and sample extraction

Blocks, seven layers high and seven beads wide, are built at a single deposition direction. The process was interrupted between each layer until the temperature of the previous layer reached less than 300 °C. The building strategy and sample extraction are illustrated in Fig. 3. The morphology, microstructure, and hardness profile of the blocks is described in [4].

The surface of the blocks shows largely shiny areas combined with dull, brown and blue areas (Fig. 4). Thirteen blocks were manufactured for the mechanical investigations described in this paper.

2.3. Post build-up heat treatment

Heat treatments were carried out before final machining of the samples to prevent contamination from the oven atmosphere. Two post build-up heat treatments were applied.

- *600 °C/4 h*: Stress-relaxation at 600 °C for 4 h followed by furnace cooling [19] to reduce residual stresses without substantial change to the microstructure [12,20]. Stress-relaxation is generally recommended after the welding of aerospace components [21].
- *1200 °C/2 h*: β-solution heat treatment at 1200 °C for 2 h followed by furnace cooling. This heat treatment is typically not applied in aerospace, but was performed, according to [22], to investigate microstructural and mechanical effects. The treatment dissolves the columnar prior β-grain morphology and creates equiaxed prior β-grains which are shown in [4,22].

2.4. Mechanical characterization

In order to test the mechanical properties in the deposition direction (x-direction), samples (SF10a) were extracted according to Fig. 3b. The tests were performed on a Zwick Z250 (displacement controlled at 3 mm/min) at room temperature according to european standard EN 10002 [23]. The properties in *z*-direction were tested by punch samples (So11c), which were extracted according to Fig. 3c. Traditional tensile samples could not be

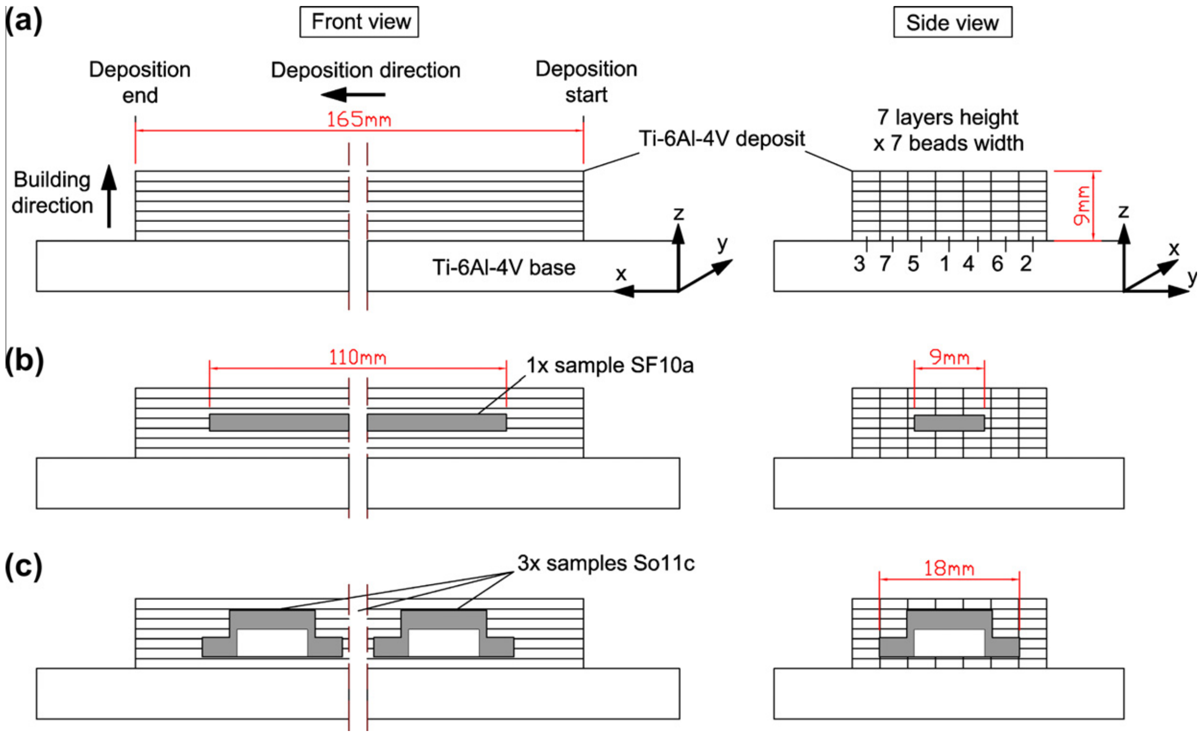

Fig. 3. Schematic drawing of the Ti–6Al–4V blocks built by wire-feed deposition: (a) building strategy (digits at the side view indicate the deposition sequence of the beads within a layer); (b) location of extraction of static tensile samples – one sample from each block; (c) location of extraction of punch samples – three samples from each block.

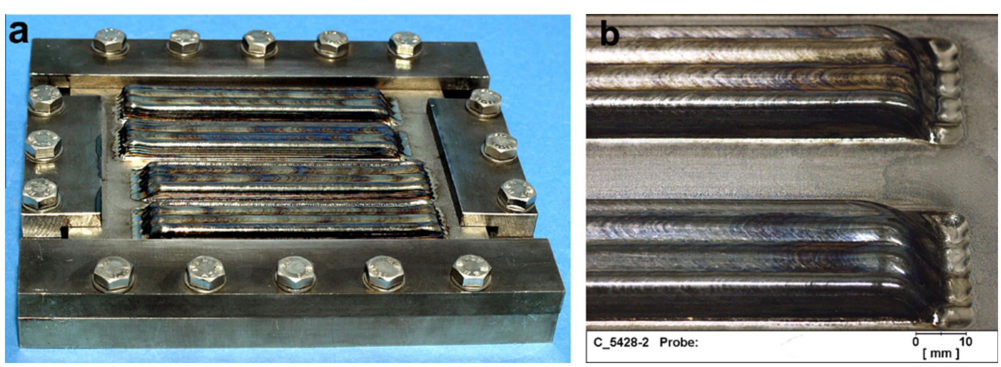

Fig. 4. Exemplary Ti–6Al–4V blocks built by wire-feed deposition: (a) the Ti–6Al–4V base is clamped during the deposition to avoid its distortion; (b) detailed view of the endings of the blocks.

Sample	Test direction	Drawing
"SF10a" Static tensile sample	Deposited blocks: x Plate: Longitudinal (L), Long transverse (LT)	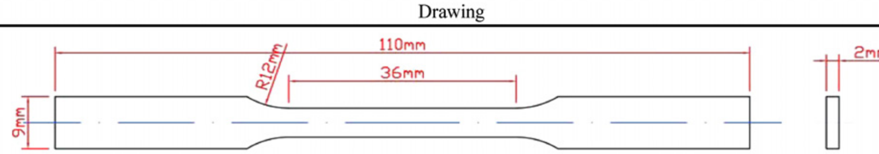
"So11c" Punch sample	Deposited blocks: z Plate: Short transverse (ST)	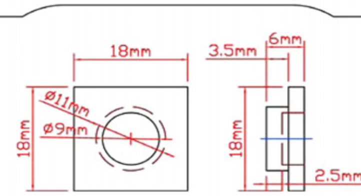

Fig. 5. Static tensile samples (SF10a) and punch samples (So11c) which are extracted from the deposited Ti–6Al–4V blocks for testing of mechanical properties.

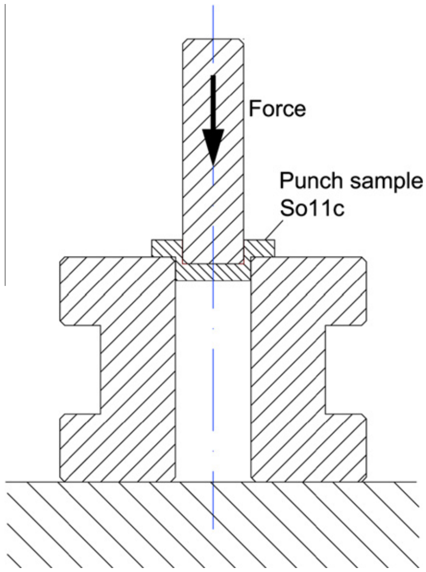

Fig. 6. Schematic drawing of the punch test: the force to failure is an approximate measure for the ultimate tensile strength in short-transverse-direction (Ti–6Al–4V plate) or *z*-direction (Ti–6Al–4V blocks).

extracted in the *z*-direction due to the low height of the blocks. Designation and geometry of the samples are illustrated in Fig. 5.

Thirteen samples of SF10a (from 13 blocks) and eighteen samples of So11c (from six blocks) were extracted. Additionally, six samples of SF10a (three longitudinal, three long traverse) and five samples of So11c were extracted from the (heat unaffected) base plate. The punch samples were tested on a Zwick Z1747 (displacement controlled at 0.5 mm/min) at room temperature according to Fig. 6. The force to failure of a punch sample is an approximate measure for the ultimate tensile strength. Due to the shape of the samples, however, a multiaxial state of stress (notch effect) is expected.

All samples were analysed by X-rays. According to Military Specifications and Standards (MIL-STD-453) 1T hole [24], porosity was not detected, suggesting a fully consolidated material in any sample.

2.5. Chemical characterization

The metallic elements were determined by X-ray fluorescence analysis (XRFA) using a PW2404/4 kW (Panalytical) equipment. The gases hydrogen (H), nitrogen (N) and oxygen (O) as well as the non-metal carbon (C) are determined by carrier gas hot extraction. Oxygen and nitrogen are determined by a TC436Ar (Leco), hydrogen by an OH-900 (Eltra), carbon by a C/S300 Modell 777-900-400 (Leco). An oxygen-equivalent for titanium can be calculated to [25,26]:

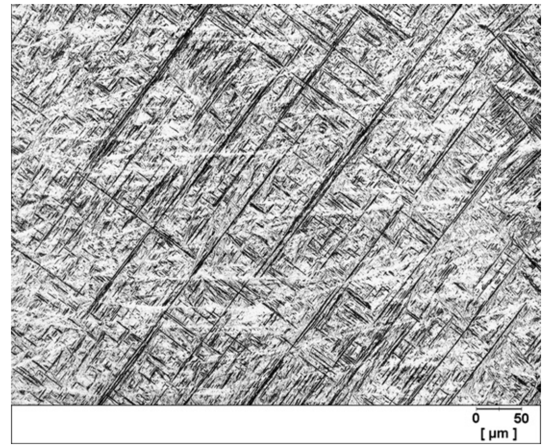

Fig. 7. Typical microstructure of a Ti–6Al–4V block (*y–z* plane) in as-built or 600 °C/4 h condition produced by the parameter set P38/P58 (laser power 3.5/2.625 kW, deposition speed 10/7.5 mm/s, wire-feed speed 40/30 mm/s): fine lamellar α + β-phase; the rectangular grid structure in a few areas suggests martensitic α [28,29].

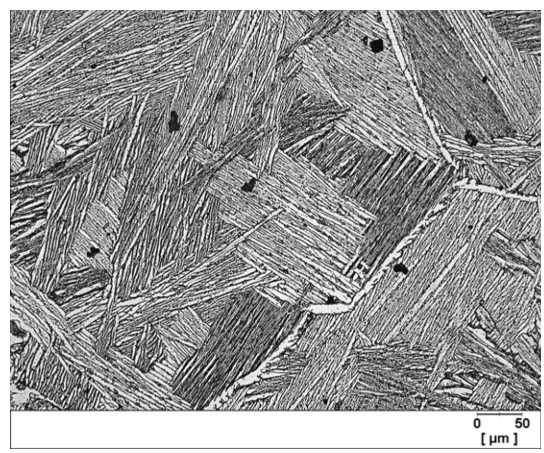

Fig. 8. Typical microstructure of a Ti–6Al–4V block (*y–z* plane) in the 1200 °C/2 h condition produced by the parameter set P38/P58 (Laser power 3.5/2.625 kW, deposition speed 10/7.5 mm/s, wire-feed speed 40/30 mm/s): colony α-phase (bright phase) within prior β-grains that are decorated by grain boundary α.

$$O_{eq} = O + 2 \cdot N + 2/3 \cdot C \text{ (all in wt.\%)} \quad (1)$$

2.6. Microstructural characterization

Samples were cold mounted in an EpoFix resin and polished with SiC paper (80, 220, 800, 1200, 2400 grit) in a RotoPol 31 machine (Struers). After etching for 15–30 s using 18% HCl (hydrochloric acid) + 11% HF (hydrofluoric acid) in water, light microscopy pictures were taken with a Polyvar microscope (Reichert-Jung).

Table 3
Chemical compositions of the Ti–6Al–4V blocks deposited, the Ti–6Al–4V plate used as base, and the Ti–6Al–4V wire (ELI: extra low interstitials) used for deposition; each element was measured five times.

Chemical analysis (wt.%)	Al	V	C	H	O	N	Fe
Ti–6Al–4V block, deposited	5.98	3.90	0.005	0.0019	0.062	0.022	0.04
Standard deviation (%)	±2	±2	±15	±11	±13	±8	±4
Ti–6Al–4V ELI welding wire, used	6.00	3.91	0.010	0.0019	0.045	0.010	0.05
Standard deviation (%)	±2	±2	±7	±27	±30	±7	±1
Ti–6Al–4V plate, used	6.17	4.02	0.007	0.0064	0.135	0.011	0.15
Standard deviation (%)	±0	±0	±11	±2	±1	±13	±0

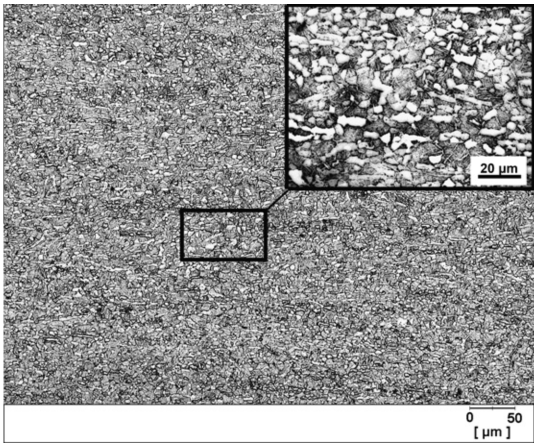

Fig. 9. Bimodal microstructure of the Ti–6Al–4V plate used as base: primary α-grains (bright phase) in a basket-weave α + β-matrix (dark phase).

3. Results

3.1. Chemical analysis

Table 3 presents the average chemical composition measured at five blocks. Furthermore, it contains the composition of the wire feedstock (ELI: extra low interstitials) and base plate used. By means of Eq. (1), the average oxygen-equivalent of a block is calculated to $O_{eq,block}$ = 0.109 wt.%, of ELI wire to $O_{eq,ELIwire}$ = 0.072 wt.%, and of the plate to $O_{eq,Plate}$ = 0.161 wt.%. Hence, the oxygen-equivalent of the wire material increased by 51% after deposition. The particular impurity levels, however, are considerably below those tolerated (O = 0.20 wt.%, N = 0.05 wt.%, C = 0.08 wt.% according to aerospace material specifications (AMS) 4911L [27]) and below the permissible oxygen-equivalent of plate material ($O_{eq,Plate,max}$ = 0.353 wt.%).

3.2. Morphology and microstructure

The mechanical properties are considered to be dominantly influenced by the significantly reduced size of the α-lamellae rather than by prior β-grains [4,13]. According to [4], the microstructures of P38 and P58 blocks are similar in the as-built and the 600 °C/4 h condition on a light microscopic level. The microstructures are analyzed by electron microscopy in [12] with a similar conclusion. The microstructure generally consists of a fine lamellar structure (mainly basket-weave, but also colony α) containing martensitic α in a few areas (Fig. 7). The microstructures of P38 and P58 block are also similar to one another in the 1200 °C/2 h condition consisting mainly of coarse colony α (Fig. 8). The microstructure of the base plate is bimodal (Fig. 9) and consists of primary α-grains in a basket-weave α + β-matrix.

3.3. Mechanical properties

3.3.1. Static tensile tests

Fig. 10 shows the stress-strain curves for the different heat treatments and parameter sets, which are compared to plate material. There is a reasonable scatter noticed, not only within one parameter set and one heat treatment. This is also observed in [12] for different kinds of deposits and smaller tensile samples. The plate material also shows a certain scatter. As expected, the material tested in the *L*-direction (longitudinal) has a higher strength and ductility than in the *LT*-direction (long traverse). The *L*-direction is parallel to the principal direction of flow in worked metal [30] and typically shows higher strength properties [31] since the grains and defects are aligned parallel. Fig. 10 shows that the work hardening, especially of as-built and 600 °C/4 h samples, is slightly higher than that of the plate material. The type of fracture can be assessed by a macroscopic inspection of the sample (Fig. 11): a more ductile fracture shows a larger amount of necking and a rougher appearance of the fracture surface than a brittle fracture [32]. However, there is no apparent relationship of ductility or strength with the angle of fracture at wire-feed ALM material (Fig. 11, side view). It can also be verified in Fig. 11 that samples

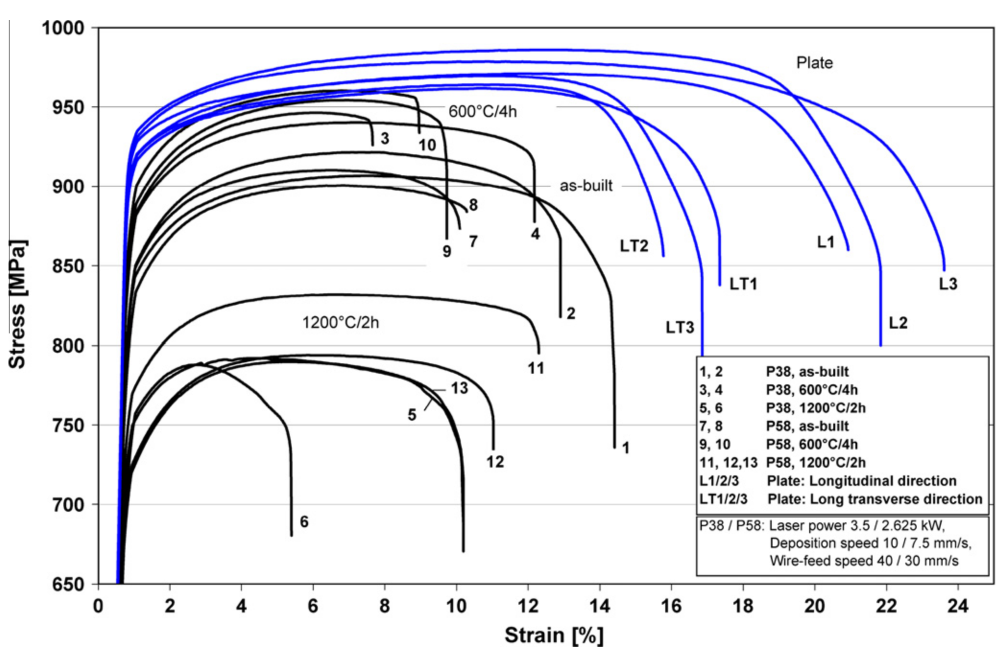

Fig. 10. Stress–strain curves of the Ti–6Al–4V plate material (as-delivered condition) and the Ti–6Al–4V blocks that were deposited by the process parameters P38 and P58 (as-built, 600 °C/4 h, and 1200 °C/2 h condition).

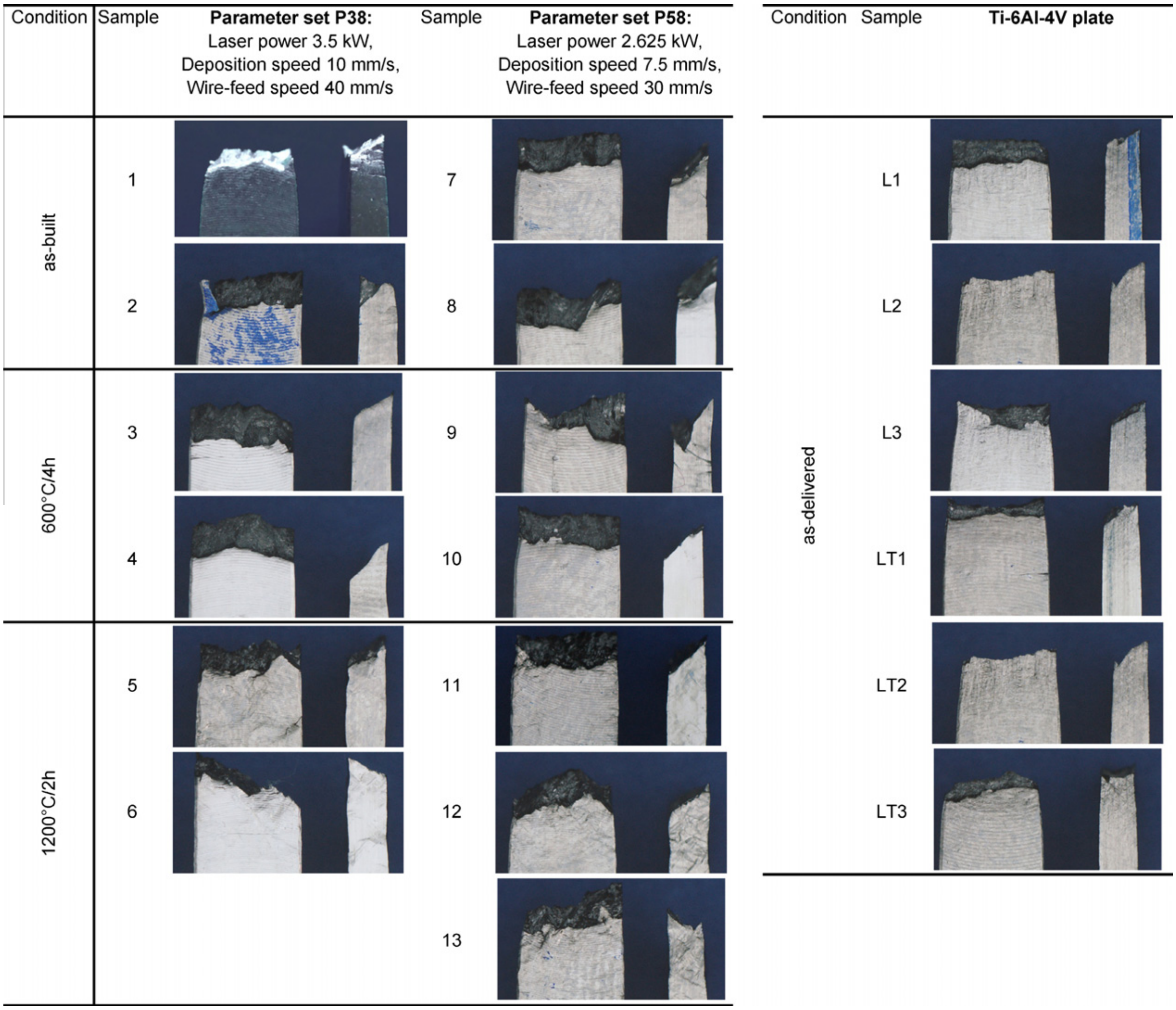

Fig. 11. Front and side view on the tested tensile samples extracted from the Ti–6Al–4V blocks that were deposited by the process parameters P38 and P58 (as-built, 600 °C/4 h, and 1200 °C/2 h condition) and from the Ti–6Al–4V plate material (as-delivered condition).

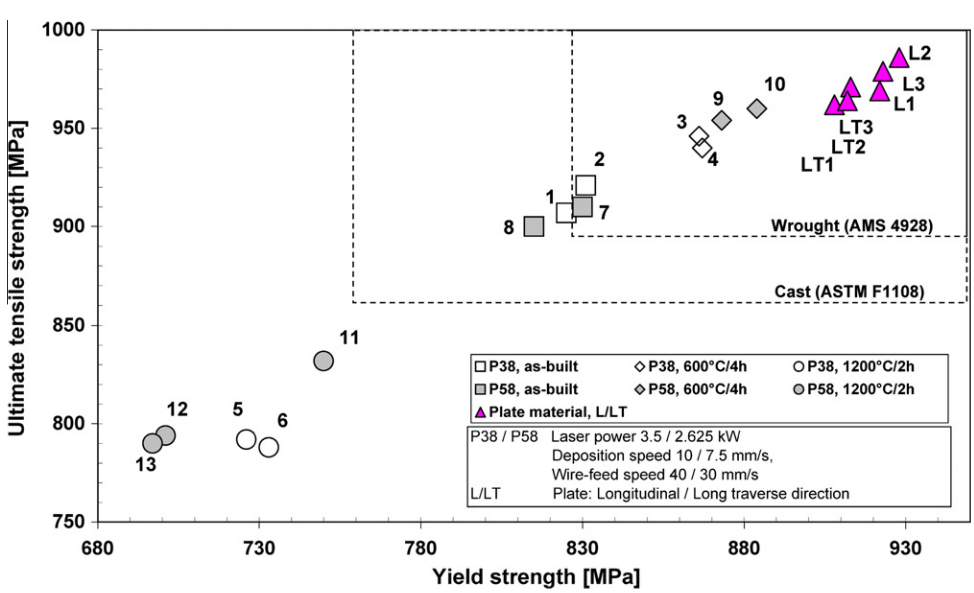

Fig. 12. Yield and ultimate tensile strength of the Ti–6Al–4V blocks deposited by process parameters P38 and P58 (as-built, 600 °C/4 h, and 1200 °C/2 h condition) in comparison with the Ti–6Al–4V plate used, wrought [34], and cast material [35]; the digits represent the sample number.

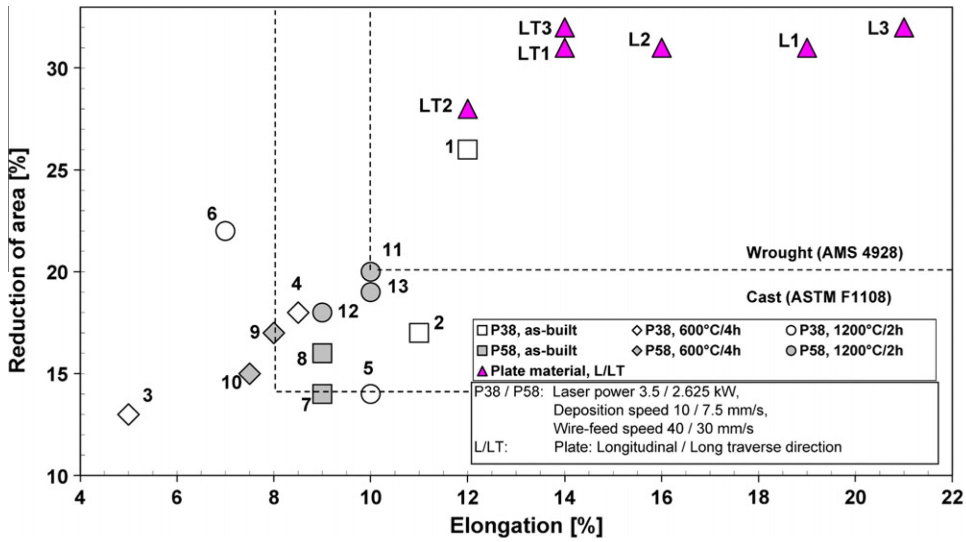

Fig. 13. Elongation and reduction of area of the Ti–6Al–4V blocks deposited by the process parameters P38 and P58 (as-built, 600 °C/4 h, and 1200 °C/2 h condition) in comparison with the Ti–6Al–4V plate used, wrought [34], and cast material [35]; the digits represent the sample number.

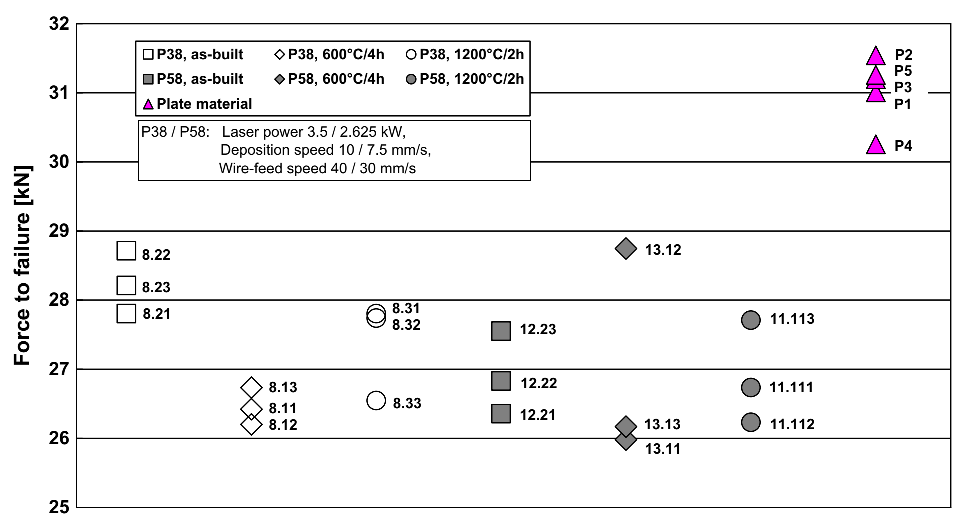

Fig. 14. Forces to failure of the Ti–6Al–4V blocks deposited by the process parameters P38 and P58 (as-built, 600 °C/4 h, and 1200 °C/2 h condition) in comparison with the Ti–6Al–4V plate used; the force to failure is an approximate measure of the ultimate tensile strength in short-transverse-direction (plate) or z-direction (blocks); the digits represent the sample number.

showing a coarse microstructure, i.e. 1200 °C/2 h samples, lose their smooth surface and become scarred according to [33].

Figs. 12 and 13 summarize strength (yield, ultimate tensile) and ductility (elongation, reduction of area) data, respectively. One P38 as-built sample achieves the properties of wrought material (AMS 4928 [34]). One P38 and two P58 as-built samples achieve at least the properties of cast material according to american society for testing and materials (ASTM) F1108 [35]. The 600 °C/4 h material shows the highest strength, but also the lowest ductility. The 1200 °C/2 h material shows a strength value below the cast material and a ductility comparable to the cast material. The P58 material shows a higher strength increase than the P38 material after the 600 °C/4 h treatment. The material produced at P38 has similar strength properties to the material built with P58. As expected, the plate material achieves the strength and ductility of a wrought material.

3.3.2. Punch tests

Fig. 14 exhibits the forces to failure for the wire-feed ALM samples and the plate material. The forces of ALM material are considerably lower than those of the plate material. The P38 material shows a greater strength than the P58 material, especially in the as-built condition. It is remarkable that the 600 °C/4 h treatment does not lead to a higher strength in the *z*-direction, contrary to the *x*-direction. In comparison to the as-built samples, the 1200 °C/2 h treatment leads to a decreased strength in the P38 samples and to a similar strength in the P58 samples.

A macroscopic observation of the punch samples tested (Fig. 15) leads to some interesting results: The P38 1200 °C/2 h samples show the roughest fracture behaviour and even considerably rougher than the P58 1200 °C/2 h samples. The plate samples show the smoothest fracture surfaces. The fracture surfaces of the P38 as-built and 600 °C/4 h samples are also smooth whereas the P58

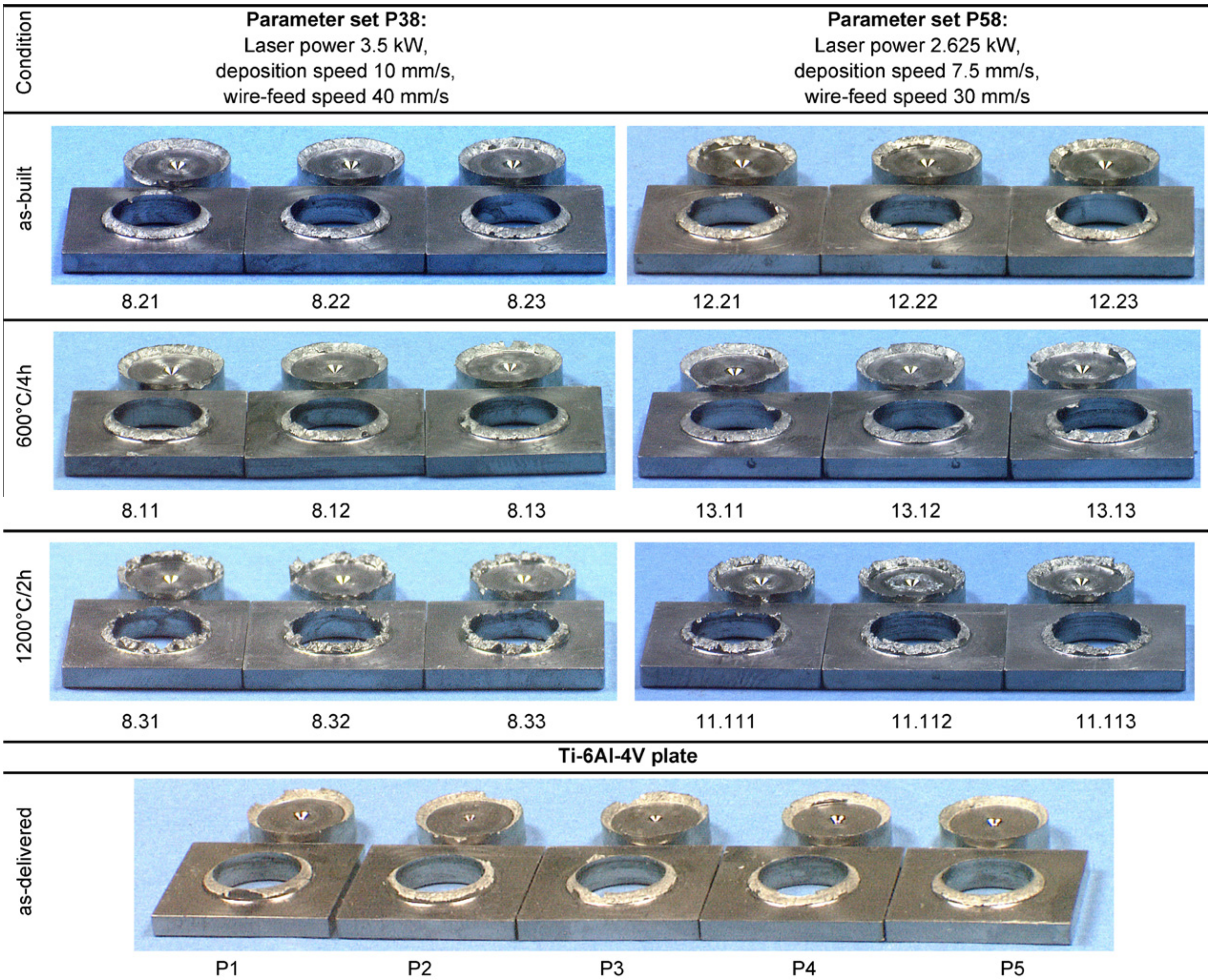

Fig. 15. Tested punch samples extracted from the Ti–6Al–4V blocks that were deposited by the process parameters P38 and P58 (as-built, 600 °C/4 h, and 1200 °C/2 h condition) and extracted from the Ti–6Al–4V plate material (as-delivered condition); the digits represent the sample number.

as-built and 600 °C/4 h samples are rougher. Similar to the tensile samples, there is no apparent relationship between force to failure or strength with the angle of fracture.

4. Discussion

The mechanical properties of Ti–6Al–4V are mainly influenced by its microstructure and chemical composition [36]. A fine or equiaxed microstructure increases strength and ductility, while a coarse or lamellar microstructure decreases strength and ductility [36,37]. Furthermore, an increasing amount of impurities increases strength but decreases elongation. For example, an increase from 0.05 up to 0.15 wt.% of oxygen results in an increase of ultimate tensile strength of around 160 MPa for pure titanium [36].

Regarding the static tensile properties, it was observed that wire-feed ALM material is competitive to cast rather than to wrought material in the as-built and 600 °C/4 h condition. One batch fulfilled the specifications of wrought material and three batches achieved at least the properties of cast material. However, the strength properties are often comparable to wrought material properties while ductility is typically lower.

Additive layer manufacturing or deposition welding is, in principle, a welding or mini-casting process characterized by heterogeneous nucleation, and directional and rapid solidification [4]. Hence, its morphology and microstructure is related to the weldments or castings. It is therefore reasonable that the mechanical properties be competitive to cast rather than to wrought material. However, the most influential microstructural parameter for the mechanical properties of lamellar microstructures is the α-colony size [38] (or α-lath thickness [39]). It determines the effective slip length in lamellar microstructures. Due to the rapid solidification and cooling during ALM processes [40], the microstructure is generally finer than for cast material [41]. Besides, a large increase in (yield) strength is observed when the colony structure changed to a martensitic type of microstructure [38], which is the case for ALM material. Altogether, this leads to a high strength, close to the properties of the wrought material. At the same time, the ductility declines with increasing martensite content [38]. Therefore, the strength properties are often comparable to the wrought material properties while ductility is lower. As expected, the plate material shows a relatively high strength and ductility. This is mainly a result of its fine equiaxed microstructure (Fig. 9). The high oxygen-equivalent compared to wire-feed ALM material (Table 3) also contributes to a higher strength [36]. It should also be considered that the microstructure of an ALM tensile sample is not as homogeneous along the y–z and x–y plane as in the wrought material. Besides strong textures [42], the microstructure is characterized by various heat affected zones [4] (e.g. layer bands [43,44]). This leads to inhomogeneous and site-dependent properties (see also hardness profile in [4,12]). The tensile samples were extracted from similar locations in the blocks. However, slight variations in microstructure and location of the heat-affected zone might result in the data scatter observed. This is also the case for the punch samples. For future applications, it can therefore be very important to apply a homogenizing post heat treatment to reduce the scattering.

It was further observed that the 600 °C/4 h treatment leads to highest strength and to lowest ductility, at least in the deposition direction. In contrast to the tensile samples, the punch samples showed a lower strength after a 600 °C/4 h treatment.

With respect to the potential hardening mechanisms [38], the most reasonable – or only possible – mechanism to explain the strength increase is precipitation hardening. The hardness increase of the ALM blocks after a 600 °C/4 h treatment (average Vickers hardness: 327 HV0.5 → 342 HV0.5 [4]) supports this suggestion.

Precipitation hardening of the α-phase occurs by coherent Ti_3Al (α_2) particles [36,38,45]. Upon annealing in the α + β-region, significant alloy element partitioning takes place and the α-phase is enriched in α-stabilizing elements (Al, O, Sn) and substantial volume fractions of coherent Ti_3Al particles can be precipitated in the α-phase by aging, for example, at 500 °C (Ti–6Al–4V) [38]. In [36], aging temperatures of 500–600 °C are reported for Ti–6Al–4V containing less than 0.2 wt.% oxygen. At high aging temperatures, ordering should not be expected, as oxygen would have a high jump frequency. The relatively low oxygen content (0.062 wt.%, Table 3) in the blocks supports the theory of Ti_3Al precipitation. In contrast, it is noted in [38] that the Ti_3Al solvus temperature is approximately 550 °C and a heat treatment at 600 °C or above will only be a stress-relaxation treatment. Further aging temperatures found in literature are usually below 600 °C, e.g. Ti_3Al precipitation after 540 °C/2 h [46] or 538 °C/4 h [29]. Nevertheless, according to [47], Ti_3Al precipitation is slow and the influence of cooling speed is strong. Fast cooling after aging leads to higher strength loss than slow furnace cooling. For maximum strength, slow furnace cooling until 400 °C is required [47]. Therefore, during the slow heating and furnace cooling applied by the 600 °C/4 h treatment, the material is, at least for a certain time, in the temperature region of precipitation hardening. According to [19,20], a 600 °C/4 h treatment can also be considered as an aging treatment to produce precipitations leading to an increase in strength, which can be applied to some solution-treated and water-quenched titanium alloys [20]. According to [38], Ti_3Al precipitation not only increases yield strength, but also reduces breaking elongation. This was also observed in [29]: In nine out of twelve cases a subsequent aging treatment at 538 °C/4 h (furnace-cooled) increased in strength and, in nine cases, decreased in ductility. However, a ductility increase after aging is also reported. In [45], a 545 °C/200 h (furnace cooled) treatment increased static and dynamic strength and ductility at a Widmannstätten and equiaxed type of microstructure. In [48], a 640 °C/2 h treatment increased strength and elongation in powder-feed ALM material. However, it should be noted that the temperature of 640 °C is considered too high for Ti_3Al precipitation. Strength and ductility may be increased in [48] due to lower unfavourable residual stresses after aging. So in conclusion, an aging treatment might be a potential treatment to increase strength, however, it does not reduce the scatter.

Regarding the punch samples, there is no evident reason at first glance why precipitation hardening should not increase the force to failure in building direction (z-direction). The shape of the punch samples (Fig. 6), however, does not lead to a homogeneous, uniaxial state of stress. The samples therefore embody notched samples, i.e. samples having a stress concentration factor $K_t > 1$.

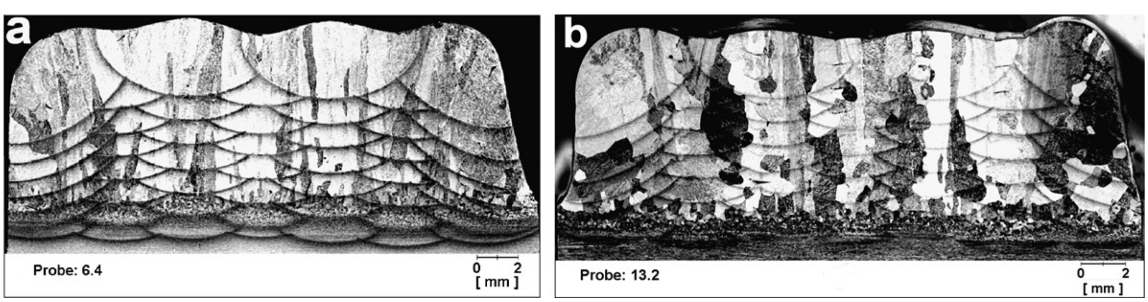

Fig. 16. Macrostructure of exemplary Ti–6Al–4V blocks (y–z plane) that were deposited by the process parameter set P38 (laser power 3.5 kW, deposition speed 10 mm/s, wire-feed speed 40 mm/s): (a) as-built condition; (b) 600 °C/4 h condition.

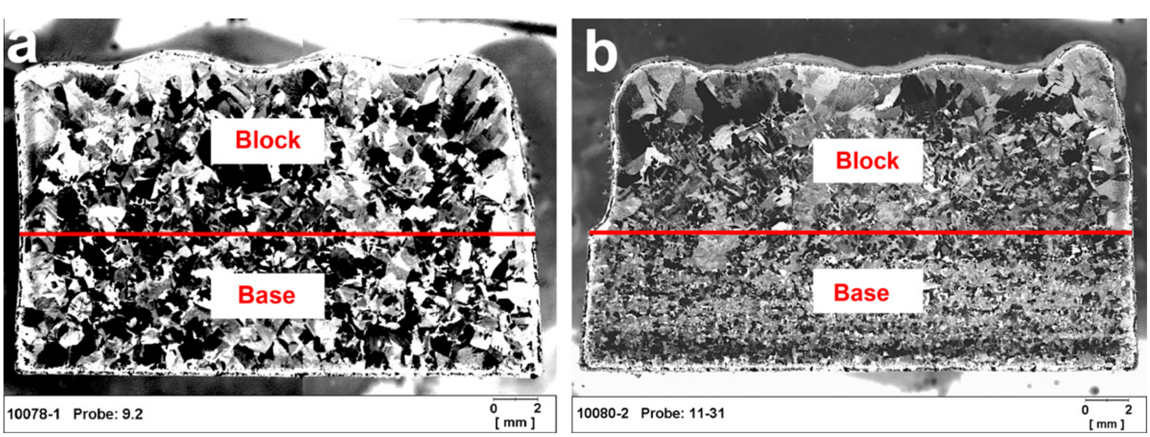

Fig. 17. Macrostructure of Ti–6Al–4V blocks (y–z plane) in 1200 °C/2 h condition that were deposited by process parameter set (a) P38 (Laser power 3.5 kW, deposition speed 10 mm/s, wire-feed speed 40 mm/s), (b) P58 (laser power 2.625 kW, deposition speed 7.5 mm/s, wire-feed speed 30 mm/s).

Brittle materials tend to be more sensitive to notches than ductile materials as ductile materials can reduce the peak stresses by plastic deformation [49,50]. It is therefore reasonable that the 600 °C/4 h hardened samples show a reduced force to failure compared to the as-built samples (Fig. 14). This is in line with the observation that even the 1200 °C/2 h material shows a higher force to failure than the 600 °C/4 h material.

It was observed that the 1200 °C/2 h treatment generally tends to decrease strength in the deposition direction. Furthermore, the surface of the 1200 °C/2 h tensile samples became scarred and the punch samples showed the roughest fracture behaviour after testing.

The microstructures of as-built, 600 °C/4 h, and 1200 °C/2 h blocks are shown in Figs. 7 and 8. The as-built and 600 °C/4 h blocks show a macrostructure of columnar prior β-grains that are growing epitaxially across many layers and opposite to the heat flow (Fig. 16). This macrostructure is similar for the P38 and P58 blocks. The development and details of the macrostructure are described elsewhere [4].

In contrast to the as-built and 600 °C/4 h blocks, the columnar prior β-grain structure is eliminated and replaced by equiaxed prior β-grains at the 1200 °C/2 h blocks (Fig. 17). This was also observed in [22] after a 1200 °C/2 h treatment. It is no longer possible to distinguish between the base and deposited material by means of the microstructure. At 1200 °C, the $\alpha + \beta$ microstructure at room temperature (Fig. 7) is completely β and the martensitic structures, dislocations, and residual stresses are eliminated due to the high diffusion rate and low yield strength. Due to slow furnace cooling, large α-colonies are created, which is expected after a heat treatment above T_β followed by furnace cooling [36]. The blocks built with P38 (Fig. 17a), however, show on average larger grains and a more homogeneous size distribution compared to the blocks built with P58 (Fig. 17b).

The coarse grains (Fig. 17) and coarse lamellae (Fig. 8) explain the reduced strength of 1200 °C/2 h samples in deposition direction (Fig. 12) as well as the scarred surfaces and rough fracture behaviour (Figs. 11 and 15). Due to the overall reductions in boundaries and dislocations, the strength of Ti–6Al–4V is decreased [38]. As the prior β-grains are on average smaller at the P58 blocks (Fig. 17b) than at the P38 blocks (Fig. 17a), the higher force to failure of P58 samples in 1200 °C/2 h condition (Fig. 14) can also be explained. A further explanation of directional variance in as-built and heat treated condition might be the anisotropy of crystallographic texture in the deposits [42,51]. The 1200 °C/2 h treatment might eliminate such textures. However, the effect of texture on properties is not straightforward and requires further investigation.

5. Conclusions

In this paper, static tensile and punch samples that were extracted from additive manufactured Ti–6Al–4V blocks are tested. The tests are accompanied by chemical analysis and microstructural investigations. The results are evaluated with respect to the Ti–6Al–4V plate material used as base and aerospace material specifications.

Depending on the building parameter set and post heat treatment, the yield strength reaches 697–884 MPa, ultimate tensile strength 790–960 MPa, elongation 5–12%, and reduction of area 13–26%. The influence of the two different building parameter sets (Laser power 3.5 kW/2.625 kW, deposition speed 10 mm/s/7.5 mm/s, wire-feed speed 40 mm/s/30 mm/s) on the mechanical properties is not as large and significant than that of the post heat treatments (as-built, 600 °C/4 h, 1200 °C/2 h).

Parallel to the deposition direction (*x*-direction), as-deposited Ti–6Al–4V can achieve yield and ultimate tensile strength, elongation, and reduction of area fulfilling the specifications of the wrought material. Nevertheless, the deposited Ti–6Al–4V material is generally competitive to cast rather than to the wrought material. The 600 °C/4 h post heat treatment leads to remarkable higher strength properties in the deposition direction (*x*-direction), but can also decrease ductility properties. The 1200 °C/2 h post heat treatment entirely annihilates the as-built macrostructure and generally leads to strength properties below that of cast material. Due to the results of this study, this heat treatment cannot be recommended for any structural applications requiring high strength and ductility.

The particular impurity levels of the deposits are considerably below the ones of the plate used and below those tolerated according to aerospace material specifications. Wire-feed deposits might therefore be also interesting for applications that require a low impurity level amongst other microstructural characteristics. Due to the observed scatter in mechanical properties, a post heat treatment is recommended, which homogenizes the microstructure and does not largely influence strength and ductility. The 600 °C/4 h and 1200 °C/2 h treatment were not useful for this purpose.

Acknowledgments

The activities at EADS Innovation Works were especially supported by Achim Schoberth, Vitus Holzinger, Christian Plander, Birgit Vetter, Elvira Reuder, Cem Dedeoglu, and Dr. Claudio Dalle Donne. The discussions and collaboration with Dr. Bernd Baufeld (NAMRC, Rotherham) were highly appreciated.

References

[1] Walner E. Titan-und Nickellegierungen – unverzichtbar im Flugzeugbau. Ingenieur-Werkstoffe, Konstruktion; 2008. p. 6–7.
[2] Peters M, Kumpfert J, Ward CH, Leyens C. Titanium alloys for aerospace applications. Adv Eng Mater 2003;5:419–27.
[3] Peters M, Leyens C. Titan und Titanlegierungen. Weinheim (Germany): Wiley VCH; 2002.
[4] Brandl E. Microstructural and mechanical properties of additive manufactured titanium (Ti–6Al–4V) using wire: evaluation with respect to additive processes using powder and aerospace material specifications. Aachen: Shaker Verlag; 2010.
[5] Wohlers TT. Wohlers report 2010. Fort Collins, Colorado: Wohlers Associates; 2010.
[6] Mok SH, Pashby IR, Segal JI, Bi G. Studies on microstructures and mechanical properties of Ti–6Al–2Sn–4Zr–2Mo produced by direct laser deposition. In: 3rd International WLT-conference on lasers in manufacturing, Munich; 2005. p. 773–6.
[7] Ader C, Brosemer M, Freyer C, Fricke H, Hennings D, Klocke F, et al. Research on layer manufacturing techniques at Fraunhofer. In: Solid freeform fabrication symposium; 2004. p. 26–37.
[8] Mok SH, Bi G, Folkes J, Pashby I. Deposition of Ti–6Al–4V using a high power diode laser and wire. Part I: investigation on the process characteristics. Surf Coat Technol 2008;202:4613–9.
[9] Mok SH, Bi G, Folkes J, Pashby I. Deposition of Ti–6Al–4V using a high power diode laser and wire. Part II: investigation on the mechanical properties. Surf Coat Technol 2008;202:3933–9.
[10] Taminger KMB. Electron beam freeform fabrication: a metal deposition apparatus to build components directly from CAD. In: International conference on metal powder deposition for rapid manufacturing. Arlington: NASA Langley Research Center; 2008.
[11] Hafley RA, Taminger KMB, Bird RK. Electron beam freeform fabrication in the space environment. American Institute of Aeronautics and Astronautics; 2008.
[12] Baufeld B, Brandl E, van der Biest O. Wire based additive layer manufacturing: comparison of microstructure and mechanical properties of Ti–6Al–4V components fabricated by laser-beam deposition and shaped metal deposition. J Mater Proc Technol 2011;211:1146–58.
[13] Baufeld B, van der Biest O, Gault R. Additive manufacturing of Ti–6Al–4V components by shaped metal deposition: microstructure and mechanical properties. Mater Des 2010;31:106–11.
[14] Almeida PMS, Williams S. Innovative process model of Ti–6Al–4V additive layer manufacturing using cold metal transfer (CMT). In: Solid freefrom fabrication symposium; 2010.
[15] Charles C, Järvstråt N. Modelling Ti–6Al–4V microstructure by evolution laws implemented as finite element subroutines: application to TIG metal

deposition. In: 8th International conference on trends in welding research, Pine Mountain, GA, USA; 2008.
[16] Lopes G, Miranda RM, Quintino L, Rodrigues JP. Additive manufacturing of Ti–6Al–4V based components with high power fiber lasers. Virtual Rapid Manuf 2007:369–74.
[17] Stecker S, Lachenberg KW, Wang H, Salo RC. Advanced electron beam free form fabrication methods & technology: electron beam welding. American Welding Society; 2006. p. 35–46.
[18] Dring KF, Lefstad M, Jensrud O. Production of a low-cost DMD wire feedstock by direct consolidation of Ti sponge. In: TMS annual meeting & exhibition, Seattle, WA, USA; 2010.
[19] SAE Aerospace. Heat treatment of titanium and titanium alloys. AMS-H-81200A: Aerospace Material Specification; 2003.
[20] Deutsche Norm. Wärmebehandlung von Titan-Knetlegierungen. DIN 65084: Deutsches Institut für Normung; 1990.
[21] US Department of Defense. In: Department of Defense, editor. Military handbook: titanium and titanium alloys, USA; 1974.
[22] Kelly SM. Thermal and microstructure modeling of metal deposition processes with application to Ti–6Al–4V. PhD thesis, Virginia Polytechnic Institute and State University; 2004.
[23] Deutsche Norm. Metallische Werkstoffe – Zugversuch – Teil 1: Prüfverfahren bei Raumtemperatur. DIN EN 10002-1: Deutsches Institut für Normung; 2001.
[24] Military Specifications and Standards. MIL-STD-453C – radiographic inspection; 1984.
[25] Conrad H, Doner M, De Meester B. Titanium science and technology. New York: Plenum Press; 1973.
[26] Harwig DD, Ittiwattana W, Castner H. Advances in oxygen equivalent equations for predicting the properties of titanium welds. Weld J 2001;80:126–36.
[27] SAE Aerospace. Titanium alloy, sheet, strip, and plate 6Al–4V annealed. AMS 4911L: Aerospace Material Specification; 2007.
[28] Lampman S. ASM handbook: properties and selection: nonferrous alloys and special-purpose materials. Materials Park (OH): ASM International; 1990.
[29] Titanium RMI. Facts about the metallography of titanium. Niles (USA): RMI Titanium; 1981.
[30] US Department of Defense. Military handbook: room-temperature design properties; 1998. p. 9–18 to 9–64.
[31] US Department of Defense. Military handbook: alpha–beta titanium alloys; 1998. p. 5–51 to 5–93.
[32] Callister Jr WD. Fundamentals of materials science and engineering. 5th ed. John Wiley & Sons; 2001.
[33] Bargel H-J, Schulze G. Werkstoffkunde. Berlin: Springer; 2000.
[34] SAE Aerospace. Titanium alloy bars, wire, forgings, rings, and drawn shapes 6Al–4V annealed. AMS 4928R: Aerospace Material Specification; 2007.
[35] ASTM international. Standard specification for titanium–6aluminum–4vanadium alloy castings for surgical implants (UNS R56406). F 1108-04: ASTM International; 2004.
[36] Welsch G, Boyer R, Collings EW. Materials properties handbook: titanium alloys. 2nd ed. Materials Park (Ohio): ASM International; 1998.
[37] Leyens C, Peters M. Titanium and titanium alloys: fundamentals and applications. Weinheim: Wiley-VCH; 2003.
[38] Lütjering G, Williams JC. Titanium. Berlin (Heidelberg), New York: Springer; 2003.
[39] Charles C. Modelling microstructure evolution of weld deposited Ti–6Al–4V. Licentiate thesis, Lulea University of Technology, Sweden; 2008.
[40] Wang L, Felicelli S. Influence of process parameters on the phase transformation and consequent hardness induced by the LENS process. In: TMS annual meeting & exhibition, Orlando, FL, USA; 2007.
[41] Jovanovic MT, Tadic S, Zec S, Miskovic Z, Bobic I. The effect of annealing temperatures and cooling rates on microstructure and mechanical properties of investment cast Ti–6Al–4V alloy. Mater Des 2006;27:192–9.
[42] Baufeld B, van der Biest O, Dillien S. Texture and crystal orientation in Ti–6Al–4V builds fabricated by shaped metal deposition. Met Mater Trans A 2010;41A:1917–27.
[43] Kelly SM, Kampe SL. Microstructural evolution in laser-deposited multilayer Ti–6Al–4V builds: Part I. Microstructural characterization. Met Mater Trans A 2004;35A:1861–7.
[44] Kobryn PA, Semiatin SL. The laser additive manufacture of Ti–6Al–4V. JOM 2001;53:40–2.
[45] Lee D-G, Lee S, Lee CS. Quasi-static and dynamic deformation behavior of Ti–6Al–4V alloy containing fine alpha$_2$-Ti$_3$Al precipitates. Mater Sci Eng 2004;A366:25–37.
[46] Murakami Y. Phase transformation and heat transport. In: 4th International conference on titanium, Kyoto, Japan; 1980. p. 153–67.
[47] Kellerer H. Übersicht über die Wärmebehandlung von TiAl6V4. Härterei-Technische Mitteilungen; 1970.
[48] Kelbassa I. Qualifizieren des Laserstrahl-Auftragschweißens von BLISKs aus Nickel- und Titanbasislegierungen. Dissertation, RWTH Aachen; 2006.
[49] Tóth L. Notch effect and brittle–ductile transition. Mater Sci 1998;34:619–29.
[50] Läpple V. Kerbwirkung. Einführung in die Festigkeitslehre: Vieweg + Teubner; 2008. p. 138–53.
[51] Kobryn P, Semiatin S. Microstructure and texture evolution during solidification processing of Ti–6Al–4V. J Mater Proc Technnol 2003;135:330–9.